Received: 14 August 2018 | Revised: 12 September 2018 | Accepted: 10 October 2018

DOI: 10.1002/aoc.4680

FULL PAPER

WILEY Applied Organometallic Chemistry

Synthesis, Structures and Various Biological Applications of New Zn(II) Complexes Having Different Coordination Modes Controlled by the Drug Furosemide in Presence of Bioactive Nitrogen Based Ligands

Ghana Raymoni | Hijazi Abu Ali

Department of Chemistry, Birzeit University, West Bank, Palestine

Correspondence
Hijazi Abu Ali, Department of Chemistry, Birzeit University, P.O. Box 14, West Bank, Palestine.
Email: habuali@birzeit.edu; habuali1@yahoo.com

Novel Zn(II) complexes with the general formula: $[Zn(furo)_2(L)_n]$, $n = 1$ or 2, (furo = furosemide = (4-chloro-2-(furan-2-ylmethylamino)-5-sulfamoylbenzoic acid) were prepared. The complexes $[Zn(furo)_2(MeOH)_2]$ (**1**; MeOH = methanol), $[Zn(furo)_2(2\text{-ampy})_2]$ (**2**; 2-ampy = 2-aminopyridine), $[Zn(furo)_2(2\text{-ammepy})_2]$ (**3**; 2-ammepy = 2-aminomethylpyridine), $[Zn(furo)_2(H_2O)(2,2\text{-bipy})]$ (**4**; 2,2′-bipy = 2,2′-bipyridine), $[Zn(furo)_2(H_2O)(4,4'\text{-bipy})]$ (**5**; 4,4′-bipy = 4,4′-bipyridine), $[Zn(furo)_2(1,10\text{-phen})]$ (**6**; 1,10-phen = 1,10-phenanthroline), $[Zn(furo)_2(2,9\text{-dmp})]$ (**7**; 2,9-dmp = 2,9-dimethyl-1,10-phenanthroline), and $[Zn\ (furo)_2(quin)_2]$ (**8**; quin = quinoline) were synthesized and characterized using different techniques such as IR, UV–Vis, ^{1}H NMR, ^{13}C NMR, LC/MS and others. The crystal structure of complex (**4**) was determined using single-crystal X-ray diffraction.

The anti-bacterial activity of complexes (**1**–**8**) was tested using agar diffusion method against three gram-positive (*Staphylococcus aureus, Bacillus subtilis* and *Staphylococcus epidermidis)* and three gram-negative bacteria (*Escherichia coli, Proteus mirabilis, Pseudomonas aeruginosa*). The obtained results showed different Inhibition Zone Diameters (IZD) with various anti-bacterial activities against the selected gram-positive and gram-negative bacteria.

In addition, the rate of bis-(4-nitrophenyl) phosphate hydrolysis was measured at different temperatures, different pH values and different concentrations. The rates for the eight complexes were in the following order: complex **4** > **2** > **5** > **8** > **7** > **6** > **3** > **1**.

KEYWORDS

anti-bacterial activity, bioactive nitrogen based ligands, bis-(4-nitrophenyl) phosphate, furosemide, zinc(II) complexes

1 | INTRODUCTION

Living organisms demand chemical elements for their daily life processes. These elements exist in all body tissues and fluids and their presence is essential to maintain certain physicochemical processes which are important in life.[1]

Metal ions play important roles as electrophiles in about one third of enzymes and can perform many functions.[2] The positive charge makes metal ions capable of

forming bond or charge–charge interaction with another atom. Since metal ions have a large ionic volume and high positive charge, they can associate with many ligands around them at the same time.[2]

Zinc is the second essential trace element after iron in the human body with recommended daily intake of is 12 mg/day for women, 15 mg/day for men and 7–11 mg/day for children.[3] Also it is present in plant, animal tissues and all living cells.[1] Its total quantity ranges from two to three grams with most abundance in muscles, liver, kidneys, bones, prostate and eyes.[3–5]

The body requires zinc to develop and activate T-lymphocytes.[5] Zinc deficiency due to inadequate zinc intake or absorption depresses immune system functions, can impair macrophage, can act as natural killer for cell and its complement activity.

Schiff bases are characterized as bidentate, tridentate, tetradentate and polydentate ligands. If these ligands contain functional groups such as -OH, -NH_2, -SH, they can form stable complexes with transition metal ions.[6]

When the N-ligands are attached with metal ions, they form strong σ-donors but their Π-character depends on the frameworks. In addition to N-, O-, S- and P-ligands also exist, where O-ligands classified as hard but S- and P- ligands are considered soft based on hard-soft acid base Pearson's scale.[6,7]

Based on the nature of the N- heterocycles ligands and the type of metal ion, anti-bacterial, anti-fungi, anti-microbial and anti-tumor agents have been synthesized.[6,8,9] In general these complexes show stronger anti-microbial activity than the organic ligands.[8] When these ligands contain more than two donor atoms or two or more aromatic nitrogen heterocycles into one molecule, they can form numerous chelating and bridging ligands.[6] Carboxylic acid complexes continue to receive great attention since the 19th century due to their ability to act as ligands and as anti-microbial agents in foods, drugs, anti-bacterial and anti-inflammatory drugs.[10,11]

Zinc carboxylates have wide applications in biochemical systems, catalysis, separation, sorption, non-linear optical properties and material chemistry.[12–15] Recently, many zinc carboxylate compounds with various biological activities have been synthesized and fully characterized.[16–25] Ibuprofen and 2,2′-bipyrdine zinc compounds showed anti-bacterial activity and zinc methoxyacetic acid with 1,10-phenantheoline complex also showed anti-bacterial activity.[26–30]

Furosemide, commercially known as Lasix –chemical structure is shown in Figure 1- white microcrystalline powder which is slightly soluble in water, chloroform, ethanol, and diethyl ether, but it is soluble in aqueous solutions with a pH above 8, acetone, methanol, and dimethylformamide.[31–33]

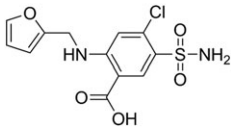

FIGURE 1 The chemical structure of Furosemide

Furosemide is extensively used in human and veterinary medicine as a potent diuretic for the treatment of edema associated with congestive heart failure and hypertension, oliguria, and asthma. In addition, furosemide and other diuretic agents show *in vitro* anti-oxidant activities.[31–36] When metals interact with ligands containing -SO_2 and NH_2 groups such as furosemide, the obtained complexes indicate interesting chemical, structural, pharmaceutical, and biological properties.[37] Silver, copper, zinc and iron are metals which form complexes with furosemide for different purposes. For example, silver-furosemide complexes showed anti-bacterial activity against Gram-positive such as *Staphylococcus aureus* and Gram negative such as *Escherichia coli* and *Pseudomanas aeruginosa*.[38] The complexation of furosemide with copper(II) and Fe(III) chloride were also used for the determination of furosemide content.[39–42]

Phosphate esters play different important roles in biological processes, such as information storage and utilization of (DNA/RNA), cellular signaling communication and energy transduction (ATP). In addition, phosphate esters have been used as pesticides for many decades.[43,44]

Hydrolysis of phosphate esters have various essential roles in biological processes, in chemistry and in biochemistry fields.[45,46] Bis(4-nitrophenyl phosphate (BNPP) is a type of phosphodiester compound that can be used as an example to study the cleavage or the formation of P-O bonds, but the hydrolysis of this compound and other types of phosphate esters is difficult and complicated due to the high stability of these compounds and high resistance to hydrolytic cleavage. The BNPP molecule has half life time ($t_{1/2}$) of 2000 years in water at 20 °C and 53 years in water at 50 °C.[43,47,48]

Because of the high stability of these compounds, scientists developed highly reactive artificial enzymes that speed up the hydrolysis of phosphate esters under physiological conditions.[44,47,49] Many studies in recent decades have shown that Mn(III), Cu(II), Zn(II), Ni(II), Fe(III), Co(III) and Ln(III) metal complexes with Schiff base ligands can act as potent catalysts to hydrolyze the phosphate esters rapidly. These metal ions may perform many functions such as activation of the phosphate group, nucleophilic molecules and stabilization of the penta-coordinate phosphorus transition state.[47,48,50,51]

Different studies showed that the spontaneous reaction for the hydrolysis of a phosphodiesters bond under

physiological conditions is first order with an approximated rate constant (k) of $1*10^{-11}$ s^{-1} and $1*10^{-10}$ s^{-1} for double strand and single strand DNA, respectively.[52]

These rates can be improved by changing the pH, the concentration of metal ions and controlling the temperature at 37 °C on a physiologically relevant time scale. BNPP, shown in Figure 2, is a distinctive example of phosphate esters.[53] Rapid hydrolysis of the high stable phosphate diester bond in BNPP by enzymes or catalysts containing metal ion complexes have been recently achieved.[54,55]

In this work, furosemide and various nitrogen based ligands were selected to synthesize the complexes which were characterized using different techniques and their biological activities were tested. The crystal structure of [Zn (furo)$_2$(H_2O)(2,2-bipy)] (**4;** 2,2′-bipy = 2,2′-bipyridine; furo = furosemide) is reported.

2 | EXPERIMENTAL

2.1 | Chemicals, materials and biological species

All reagents, chemicals and solvents used in the present work were purchased from Sigma-Aldrich with high purity and were used without any further purification.

2.2 | Physical measurements

Solid samples with anhydrous potassium bromide (KBr) were ground and compressed into a disc to use them for IR spectral measurements which were recorded in the 200–4000 cm^{-1} region using TENSOR II FT-IR Spectrometer (BRUKER). UV–Vis spectra were recorded using an Agilent 8453 photodiode array (PDA) spectrophotometer in the 200–600 nm region using CH_3OH (MeOH) as a solvent. NMR spectra were recorded using a Varian Unity Spectrometer operating at 300 MHz for ^1H and ^{13}C nucleus. Melting points were determined using capillary tubes with Electrothermal apparatus, and X-ray analyses were performed using SMART APEX CCD X-ray diffractometer (Bruker, Ettlingen, Germany).

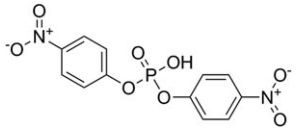

FIGURE 2 The chemical structure of BNPP ($C_{12}H_9N_2O_8P$)

2.3 | Synthesis and characterization of zinc furosemide complexes

All zinc furosemide complexes were prepared at room temperature.

2.3.1 | Synthesis of [Zn(furo)$_2$(MeOH)$_2$] (1)

Sodium hydroxide (37.4 mmol, 1.5 g) was added with stirring to furosemide (37.4 mmol, 12.4 g) dissolved in 180 ml MeOH. Then zinc chloride was added (18.7 mmol, 2.5 g) to the previous solution and the whole mixture was stirred for 3.5 hr. Then the solvent was evaporated at room temperature in air and the product was extracted by dichloromethane and ether. The solvents were evaporated and the product was washed with petroleum ether to give yellow solid.

[$Zn(C_{12}H_{10}ClN_2O_5S)_2(CH_3OH)_2$] (**1**). 77% yield; m.p. = 182 °C (d); ^1H NMR ($CDCl_3$): δ (ppm) 4.43 (d, 2H, CH_2, $^3J_{H\text{-}H}$ = 5.7 Hz), 6.30 (d, 1H, CH), 6.36 (t, 1H, CH), 6.82 (s, 1H, CH), 7.14 (NH_2), 7.56 (d, 1H, CH), 8.45 (s, 1H, CH), 9.60 (NH); $^{13}C\{1H\}$-NMR ($CDCl_3$): δ (ppm) 39.08 (CH_2), 107.68 (CH), 110.88 (CH), 112.53 (CH), 113.72 (CH), 126.17 (CH), 133.88 (C), 134.03 (C), 142.88 (C), 152.38 (CH), 152.57 (C), 170.78(C=O); IR (cm^{-1}): 3303, 1605,1556, 1498, 1423, 1382, 1299, 1159, 1071, 1011, 945, 803, 738, 583, 514, 388, 270; UV–Vis (MeOH, λ (nm)): 229, 275; ESI m/z: 787 $[M + H]^+$.

2.3.2 | Synthesis of [Zn(furo)$_2$(2-ampy)$_2$] (2)

Compound (**1**) (2.7 mmol, 2.0 g) was dissolved in 35 ml MeOH and 2-ampy (5.5 mmol, 0.5 g) dissolved in minimum amount of MeOH was added to the solution of **1** with stirring, then the clear reaction mixture was stirred for an additional 3.5 hr. The solvent was evaporated then ether and petroleum ether were added and evaporated to form solid product.

[$Zn(C_{12}H_{10}ClN_2O_5S)_2(H_2NC_5H_4N)_2$] (**2**). 45% yield; m.p. = 185–190 °C (d); ^1H NMR ($CDCl_3$): δ (ppm) 4.42 (d, 2H, CH_2), 6.02 (NH_2), 6.29 (d, 1H, CH), 6.36 (t,1H, CH), 6.44 (t, 1H, CH, $^3J_{H\text{-}H}$ = 6.6 Hz), 6.47 (d, IH, CH, $^3J_{H\text{-}H}$ = 6 Hz), 6.80 (s, IH, CH), 7.36 (t, 1H, CH, $^3J_{H\text{-}H}$ = 7.6 Hz), 7.56 (d, 1H, CH), 7.89 (d, 1H, CH, $^3J_{H\text{-}H}$ = 4.5 Hz), 8.44 (s, 1H, CH), 9.80 (NH); $^{13}C\{^1H\}$-NMR ($CDCl_3$): δ (ppm) 39.08 (CH_2), 107.63 (CH), 108.91 (CH), 110.88 (CH), 112.18 (CH), 112.32 (CH), 126.03 (CH), 134.06 (C), 137.83 (C), 142.85 (C), 147.86 (CH), 152.48 (CH), 152.62 (C), 160.10 (C), 170.63 (C=O); IR (cm^{-1}): 3568, 3322, 3223, 1607, 1560, 1496, 1447, 1374, 1298, 1262, 1150, 976, 942, 803, 770, 737, 686, 582, 520, 474,

334; UV–Vis (MeOH, λ (nm)): 230, 276; ESI m/z: 911 $[M + H]^+$.

2.3.3 | Synthesis of $[Zn(furo)_2(2\text{-ammepy})_2]$ (3)

Compound (**1**) (2.7 mmol, 2.0 g) was dissolved in 35 ml MeOH, then 2-ammpy (10.9 mmol, 1.3 g) dissolved in minimum amount of MeOH was added with stirring to the previous solution. The clear reaction mixture was formed and was stirred for an additional 3.5 hr, the solution was then evaporated, ether and petroleum ether were added and evaporated to give the desired solid product.

$[Zn(C_{12}H_{10}ClN_2O_5S)_2(C_6H_8N_2)_2]$ (**3**). 28% yield; m.p. = 140–145 °C; ^{1}H NMR (DMSO, δ): 4.03 (s, 2H, CH_2), 4.40 (d, 2H, CH_2, $^3J_{H\text{-}H}$ = 5.1 Hz), 6.30 (d, 1H, CH), 6.38 (t, 1H, CH), 6.75 (s, 1H, CH), 7.38 (t, 1H, CH, $^3J_{H\text{-}H}$ = 11.7 Hz), 7.49 (d, 1H, CH, $^3J_{H\text{-}H}$ = 7.8 Hz), 7.58 (d, 1H, CH), 7.86 (t, 1H, CH, $^3J_{H\text{-}H}$ = 7.8 Hz), 8.41 (s, 1H, CH), 8.51 (d, 1H, CH, $^3J_{H\text{-}H}$ = 3.9 Hz), 10.19 (NH_2); $^{13}C\{^1H\}$-NMR (DMSO, δ): 39.08 (CH_2), 44.43 (CH_2), 107.57 (CH), 110.90 (CH), 111.95 (CH), 117.96 (CH), 122.81 (CH),123.47 (CH), 125.82 (CH), 132.95(C), 133.80 (C), 138.47 (CH), 142.87 (C), 148.38 (CH), 152.65 (CH), 152.74 (C), 156.02 (C), 170.58(C=O); IR (cm^{-1}): 3259, 2933, 2075, 1604, 1549, 1497, 1440, 1364, 1295, 1262, 1138, 943, 817, 744, 712, 683, 629, 577, 495, 408, 333, 281, 225; UV–Vis (MeOH, λ (nm)): 229, 274; ESI m/z: 940 $[M + H]^+$.

2.3.4 | Synthesis of $[Zn(furo)_2(H_2O)(2,2\text{-bipy})]$ (4)

Compound (**1**) (2.7 mmol, 2.0 g) was dissolved in 35 ml MeOH and 2,2-bipy (2.7 mmol, 0.4 g) dissolved in minimum amount of MeOH were mixed with stirring, then the clear reaction mixture was formed and was stirred for an additional 3.5 hr. The solvent was evaporated to give a solid product. Recrystallization of the complex from MeOH by slow evaporation gave single crystals suitable for X-ray determination.

$[Zn(C_{12}H_{10}ClN_2O_5S)_2(H_2O)(C_{10}H_8N_2)]$ (**4**). 51% yield; m.p. = 226–229 °C; ^{1}H NMR ($CDCl_3$): δ (ppm) 4.42 (d, 2H, CH_2, $^3J_{H\text{-}H}$ = 5.4 Hz), 6.27 (d, 1H, CH, $^3J_{H\text{-}H}$ = 3.0 Hz), 6.35 (t, 1H, CH, $^3J_{H\text{-}H}$ = 4.2 Hz), 6.84 (s, 1H, CH), 7.16 (NH_2), 7.57 (t, 1H, 2CH), 8.09 (t, 1H, 2CH), 8.46 (s, 1H, CH), 8.50 (d, 1H, 2CH, $^3J_{H\text{-}H}$ = 7.2 Hz), 8.74 (d, 1H, 2CH, $^3J_{H\text{-}H}$ = 3.6 Hz), 9.49 (NH); $^{13}C\{^1H\}$-NMR ($CDCl_3$): δ (ppm) 39.08 (CH_2), 107.69 (CH), 110.90 (CH), 112.67 (CH), 115.26 (CH), 121.72 (2CH), 126.26 (CH), 134.08 (C), 134.21 (C), 142.88 (C), 149.49 (2CH), 152.33 (CH), 152.54 (C), 171.09 (C=O); IR (cm^{-1}): 3467, 3265, 3117, 1607, 1553, 1496, 1437, 1382, 1306, 1265, 1151, 1066, 1017, 970, 947, 902, 834, 807, 755, 687, 625, 585, 510, 478, 386; UV–Vis (MeOH, λ (nm)): 230, 276; ESI m/z: 901 $[M + H]^+$.

2.3.5 | Synthesis of $[Zn(furo)_2(H_2O)(4,4\text{-bipy})]$ (5)

Compound (**1**) (2.7 mmol, 2.0 g) was dissolved in 35 ml MeOH and 4,4′-bipy (2.7 mmol, 0.4 g) dissolved in minimum amount of MeOH were mixed with stirring, then the clear reaction mixture was formed and was stirred for an additional 3.5 h. The solvent was evaporated to give a solid product.

$[Zn(C_{12}H_{10}ClN_2O_5S)_2(H_2O)(C_{10}H_8N_2)]$ (**5**). 58% yield; m.p. = 201–202 °C; ^{1}H NMR ($CDCl_3$): δ (ppm) 4.46 (d, 2H, CH_2, $^3J_{H\text{-}H}$ = 4.8 Hz), 6.31 (d, 1H, CH), 6.36 (t, 1H, CH), 6.88 (s, 1H, CH), 7.20 (NH_2), 7.56 (d, 1H, CH), 7.87 (d, 1H, 4CH, $^3J_{H\text{-}H}$ = 4.2 Hz), 8.48 (s, 1H, CH), 8.74 (d, 1H, 4CH, $^3J_{H\text{-}H}$ = 3.6 Hz), 9.35 (NH); $^{13}C\{^1H\}$-NMR ($CDCl_3$): δ (ppm) 39.08 (CH_2), 107.74 (CH), 110.91 (CH), 112.85 (CH), 122.02 (4CH), 126.42 (CH), 134.35 (C), 141.23 (C), 142.94 (C), 145.10 (2C), 150.88 (4CH), 152.22 (CH), 152.53 (C); IR (cm^{-1}): 3260, 1608, 1559, 1497, 1415, 1372, 1307, 1265, 1159, 1070, 945, 806, 739, 686, 628, 580, 511; UV–Vis (MeOH, λ (nm)): 228, 275; ESI m/z: 901 $[M + H]^+$.

2.3.6 | Synthesis of $[Zn(furo)_2(1,10\text{-phen})]$ (6)

Compound (**1**) (2.7 mmol, 2.0 g) was dissolved in 35 ml MeOH and 1,10-phen (2.7 mmol, 0.5 g) dissolved in minimum amount of MeOH were mixed with stirring and the reaction mixture was stirred for an additional 3.5 hr. The solvent was evaporated to give solid product.

$[Zn(C_{12}H_{10}ClN_2O_5S)_2(C_{12}H_8N_2)]$ (**6**). 49% yield; m.p. 191–192 °C; ^{1}H NMR ($CDCl_3$): δ (ppm) 4.38 (s, 2H, CH_2, $^3J_{H\text{-}H}$ = 5.7 Hz), 6.28 (d, 1H, CH, $^3J_{H\text{-}H}$ = 3 Hz), 6.37 (t, 1H, CH), 6.74 (s, 1H, CH), 7.09 (NH_2), 7.57 (d, 1H, CH), 7.90 (t, 1H, 2CH, $^3J_{H\text{-}H}$ = 6.1 Hz), 8.14 (d, 1H, 2CH), 8.42 (s, 1H, CH), 8.70 (d, 1H, 2CH, $^3J_{H\text{-}H}$ = 7.5 Hz), 8.99 (d, 1H, 2CH), 10.22 (NH); $^{13}C\{^1H\}$-NMR ($CDCl_3$): δ (ppm) 39.08 (CH_2), 107.57 (CH), 110.88 (CH), 111.92 (CH), 118.11 (CH), 125.06 (2CH), 125.79 (CH), 127.38 (2CH), 129.04 (2C), 132.90 (C), 133.79 (C), 141.23 (2C), 142.85 (C), 149.90 (2CH), 152.63 (CH), 152.73 (C), 170.51 (C=O); IR (cm^{-1}): 3569, 3317, 3224, 3077, 1604, 1555, 1501, 1421, 1371, 1309, 1262, 1152, 1011, 941, 805, 724, 577, 532, 473, 333; UV–Vis (MeOH, λ (nm)): 229, 272; ESI m/z: 903 $[M + H]^+$.

2.3.7 | Synthesis of [Zn(furo)$_2$(2,9-dmp)] (7)

Compound (**1**) (2.7 mmol, 2.0 g) was dissolved in 35 ml MeOH and 2,9-dmp (2.7 mmol, 0.57 g) dissolved in minimum amount of MeOH were mixed with stirring, then the reaction mixture was formed and was stirred for an additional 3.5 h. The solvent was evaporated to give solid product.

[Zn($C_{12}H_{10}ClN_2O_5S$)$_2$($C_{14}H_{12}N_2$)] (**7**). 32% yield; m.p. = 261–265 °C (d); ^{1}H NMR ($CDCl_3$): δ (ppm) 2.49 (s, 3H, $2CH_3$), 4.44 (d, 2H, CH_2, $^3J_{H\text{-}H}$ = 5.4 Hz), 6.28 (d, 1H, CH), 6.36 (t, 1H, CH), 6.90 (s, 1H, CH), 7.23 (NH_2), 7.55 (d, 1H, CH), 8.05 (d, 1H, 2CH, $^3J_{H\text{-}H}$ = 8.4 Hz), 8.14 (d, 1H, 2CH), 8.49 (s, 1H, CH), 8.80 (d, 1H, 2CH, $^3J_{H\text{-}H}$ = 8.4 Hz), 8.89 (NH); ^{13}C{^{1}H}-NMR ($CDCl_3$): δ (ppm) 24.67 ($2CH_3$), 39.08 (CH_2), 107.89 (CH), 110.93 (CH), 113.25 (CH), 126.66 (2CH), 126.83 (CH), 127.41 (2CH), 134.55 (C), 135.27 (C), 139.48 (2CH), 141.23 (C), 143.05 (2C), 152.92 (CH), 152.42 (C), 158.16 (2C), 170.26 (C=O); IR (cm^{-1}): 3398, 3313, 3222, 3072, 1628, 1585, 1499, 1420, 1350, 1257, 1165, 1071, 1008, 962, 925, 863, 758, 688, 617, 583, 550, 520, 410, 326, 266; UV–Vis (MeOH, λ (nm)): 229, 275; ESI m/z: 931 $[M + H]^+$.

2.3.8 | Synthesis of [Zn(furo)$_2$(quin)$_2$] (8)

Compound (**1**) (2.7 mmol, 2.0 g) was dissolved in 35 ml MeOH and quino (11.1 mmol, 1.4 g) dissolved in minimum amount of MeOH were mixed with stirring, then the reaction mixture was stirred for an additional 3.5 hr, the solvent was evaporated then ether and petroleum ether were added and evaporated to form solid product.

[Zn($C_{12}H_{10}ClN_2O_5S$)$_2$(C_9H_7N)$_2$] (**8**). 92% yield; m.p. = 198–199 °C; ^{1}H NMR (DMSO): δ (ppm) 4.45 (d, 2H, CH_2, $^3J_{H\text{-}H}$ = 4.5 Hz), 6.33 (d, 1H, CH), 6.36 (t, 1H, CH), 6.87 (s, 1H, CH), 7.21 (NH_2), 7.58 (m, 1H, 2CH), 7.77 (m, 1H, 2CH), 8.01 (m, 1H, 2CH), 8.37 (d, 1H, CH, $^3J_{H\text{-}H}$ = 8.1 Hz), 8.50 (NH); ^{13}C{^{1}H}-NMR ($CDCl_3$): δ (ppm) 39.08 (CH_2), 107.74 (CH), 110.91 (CH), 112.79 (CH), 121.94 (CH), 126.37 (CH), 127.04 (CH), 128.38 (C), 129.33 (C), 130.00 (2CH), 134.34 (CH), 136.55 (CH), 141.23 (C), 142.91(C), 148.12 (C), 151.03 (CH), 152.28 (CH), 152.56 (C), 171.16 (C=O); IR (cm^{-1}): 3282, 3055, 2917, 1611, 1557, 1501, 1379, 1301, 1261, 1153, 1079, 945, 806, 732, 688, 584, 549, 516, 478, 386, 280; UV–Vis (MeOH, λ (nm)): 204, 225; ESI m/z: 981 $[M + H]^+$.

2.4 | X-ray single crystal diffraction

The single crystal of **4** was attached to a glass fiber, with epoxy glue and mounted on the three-circle goniometer with χ fixed at +54.76°. X-ray intensities data of **4** were carried out at room temperature on a Bruker SMART APEX CCD X-ray diffractometer system (graphite–monochromated Mo Kα radiation λ = 0.71073 Å) and detector array of 512 * 512 Pixels (Pixel size is 120 μm) using the SMART software package.[56] The data were reduced and integrated by the SAINT program package.[57] The structure was solved and refined by the SHELXTL software package.[58] H atoms were located geometrically and treated with a riding model except the H-atoms in the water molecule. To update the background frame information, the following equation was used: B` = (7B + C)/8. Where B` is the updated pixel value, B is the background pixel value before updating and C is the pixel value through the current frame.

Crystal data and details of the data collections and refinements are summarized in Table 1.

2.5 | Anti-bacterial activity

Three gram negative bacteria (*Escherichia coli*, *Proteus mirabilis*, and *Pseudomonas* aeruginosa) and three gram positive bacteria (*Staphylococcus aureus*, *Bacillus subtilis*, and *Staphylococcus epidermidis*) were used to test antibacterial activities of the new zinc complexes.

Agar diffusion method[59] was used to test antibacterial activities of complexes (**1**–**8**) *in vitro*. The sterile saline solution was formed by dissolving 0.5 g of NaCl in 500 ml of water (0.9% of NaCl), then the solution was autoclaved. The saline solution was used to dissolve single bacterial colonies until the turbidity of the suspended cells reached to the McFarland 0.5 standard, then the bacterial inoculate were spread on the surface of Muller Hinton nutrient agar by using a sterile cotton swab. The wells (diameter = 6 mm) in the agar plate were formed by using sterile glassy borer. After that, zinc complexes which were dissolved in DMSO (concentration = 6 mg/ml) were added into respective wells in plates by using 25 μL pipette. Finally, the plates were incubated at 37 °C for 12–24 hr.[22,28]

Gentamicin and Erythromycin were used as positive control, but DMSO was used as negative standard. By measuring IZD (inhibition zone diameter) in millimeter (mm), the activities of complexes were determined also, the results were determined by calculating the average of three trials, and these results are stated as average ± standard error.[22,28]

2.6 | BNPP hydrolysis

To determine the optimum conditions of the BNPP hydrolysis, the kinetic experiments were performed in three

TABLE 1 Crystal data and structure refinements for complex **4**

Property	Complex 4
Empirical formula	$C_{35}H_{34}Cl_2N_6O_{12}S_2Zn$
Formula weight	931.07
Temperature	293(1) K
Wavelength	0.71073 Å
Crystal system	Triclinic
Space group	P-1
Unit cell dimensions	a = 11.632(2) Å α = 94.742(3)° b = 12.104(2) Å ß = 104.071(3)° c = 15.572(3) Å γ = 108.523(3)°
Volume	1985.7(6) $Å^3$
Z	2
Density (calculated)	1.557 Mg/m^3
Absorption coefficient	0.928 mm^{-1}
F(000)	956
Crystal size	0.49 x 0.29 x 0.27 mm^3
Theta range for data collection	2.13 to 27.00°
Index ranges	−14 < =h < =h, −15 < =k < =15, −19 < =1 < =19
Reflections collected	21179
Independent reflections	8415 [R (int) = 0.0223]
Completeness to theta = 27.00°	97.0%
Absorption correction	Semi-empirical from equivalents
Max. and Min. transmission	0.7878 and 0.6592
Refinement method	Full-matrix least-squares on F^2
Data/restraints/parameters	8415/0/532
Goodness-of-fit on F^2	1.004
Final R indices [I > 2sigma(I)]	R_1 = 0.0475, wR_2 = 0.1197
R indices[a] (all data)	R_1 = 0.0537, wR_2 = 0.1246
Largest diff. Peak and hole	0.902 and − 0.417e.$Å^3$

a $R1 = \sum||F_o|-|F_c||/\sum|F_o|$ and $wR_2 = \{\sum[w(F_o^2 - F_c^2)^2]/\sum[w(F_o^2)^2]\}^{1/2}$

trials, then the graphs of absorbance vs. released p-nitrophenol concentration were plotted. The best-fit graphs were chosen to determine the optimum conditions.

HEPES buffer (4-(2-hydroxyethyl)-1-piperazineeth anesulfonic acid) solutions were prepared by dissolving 50 μM of HEPES in minimum amount of deionized water, then the pH was adjusted by NaOH or HCl to obtain the required pH. After that, the BNPP was dissolved in HEPES buffer to obtain a final volume of 100 ml using 100 ml volumetric flask.[22,60,61]

Zinc (II) complexes which were prepared in DMSO solution with different concentration were used as catalysts in the BNPP hydrolysis process. The zinc complexes and BNPP solutions were placed in the water bath for 10 mins at constant temperature. Then 1.5 ml of each solution were added and mixed in a quartz cell at fixed temperature and the kinetic measurement was performed.[22,60,61] UV–Vis spectrophotometer (λ = 400 nm, Є = 13400 L/mol.cm) was used to calculate the rate of p-nitrophenol formation.

3 | RESULTS AND DISCUSSION

3.1 | Synthesis zinc furosemide complexes

1 equivalent of $ZnCl_2$ was reacted with 2 equivalents of NaOH and 2 equivalents of furosemide at room temperature to form [Zn $(furo)_2(MeOH)_2$] (**1**) as shown in Scheme 1. The obtained complex has a light yellow color with 77% yield.

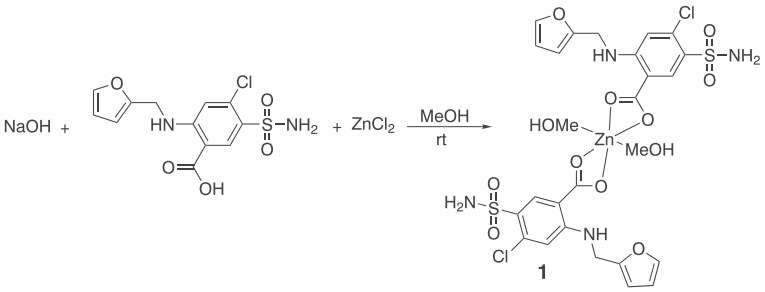

SCHEME 1 Proposed synthesis of $[Zn(furo)_2(MeOH)_2]$ (**1**)

Zinc furosemide was reacted with different molar ratios of nitrogen based ligands to form zinc furosemide complexes (**2**–**8**) as shown in Scheme 2 and Scheme 3. Table 2 shows the physical properties and the percent yields of the complexes (**1**–**8**).

3.2 | ^{1}H NMR and ^{13}C NMR

Tables S1 and S2 (supporting information) show the ^{1}H NMR and ^{13}C NMR spectral data of complex **1**, H-furo, and complex **2.** The intensities of ^{1}H NMR signals indicated good correlation with the proposed structures. In addition, the resonance chemical shifts of the parent ligands slightly shifted down field compared to the same resonances in complexes **1** and **2** which may be due to the complexation with the Zn metal cation. The O-H resonance in complexes **1** and **2** was absent which support the coordination mode with the metal center. In addition, C=O in complex **1** and complex **2** shifted downfield compared to H-furo in the ^{13}C NMR due to electron density donation (deshielding effect) from the carboxylate group in furosemide to the center of Zn(II).

Tables S3 and S5 (supporting information) show the resonance chemical shifts of the complexes (**3**–**8**). Some of the resonance chemical shifts of these complexes are slightly shifted upfield and others are shifted downfield compared to the same resonance in H-furo which may be due to the complexation with the Zn metal cation. OH group was absent in complexes possibly due to complexation with the Zn (II) center. In addition, C=O of the complexes (**3**–**8**) in ^{13}C NMR was shifted downfield compared to H-furo as shown in Tables S4 and S6 (supporting information). This downfield shift is due to the deshielding effect of carboxylate group. The intensities of ^{1}H NMR of all complexes signals showed good correlation with the proposed structures.

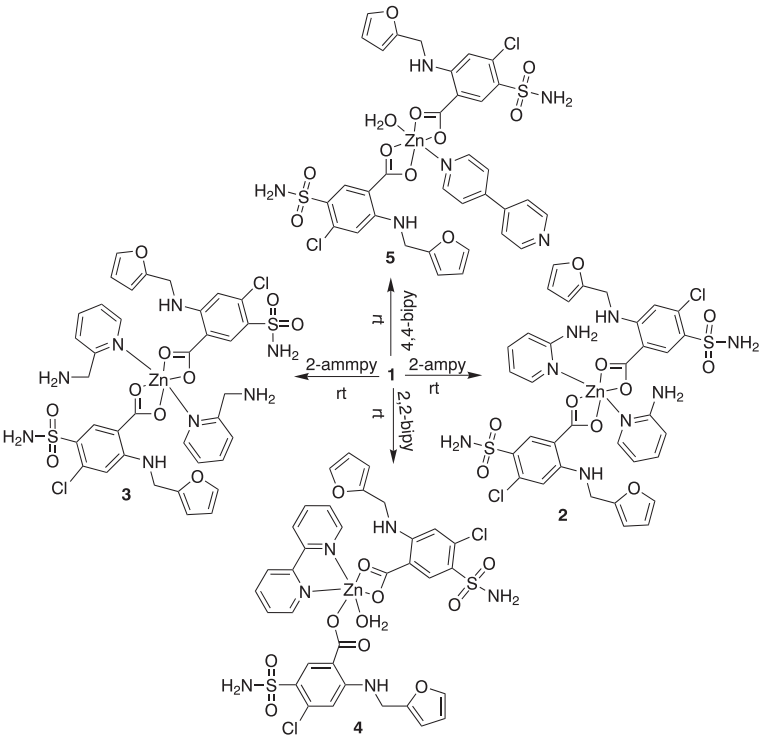

SCHEME 2 Synthesis of complexes **2**, **3**, **4** and **5**

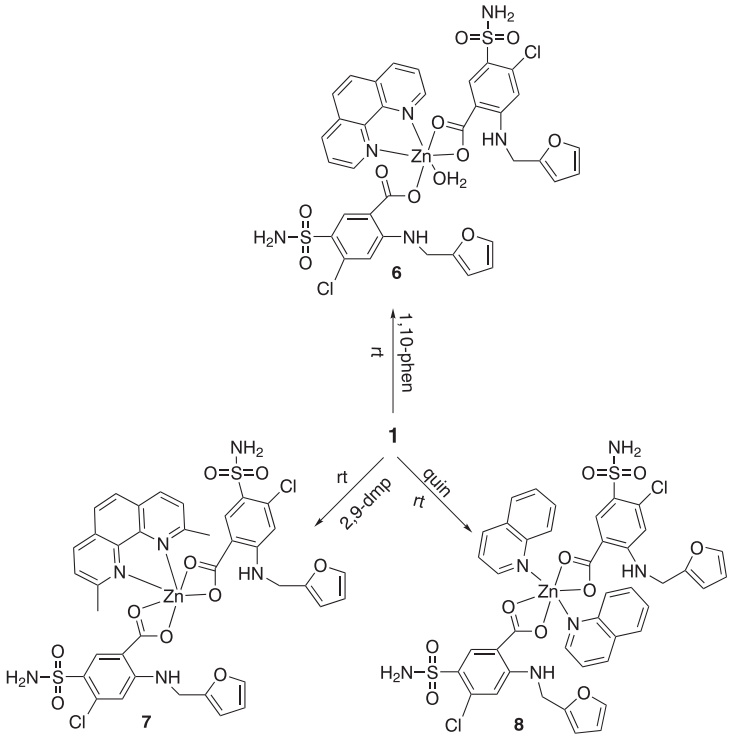

SCHEME 3 Synthesis of complexes **6**, **7** and **8**

TABLE 2 Physical properties of complexes (**1–8**) and their % yields

Complex	m.p (°C)	% Yield	Solubility
[Zn (furo)$_2$(MeOH)$_2$] (**1**)	182[d]	77	Methanol, ethanol, acetone, DMSO, DMF, slightly soluble in $CHCl_3$
[Zn (furo)$_2$(2-ampy)$_2$] (**2**)	185-190[d]	45	Acetone, DMSO, slightly soluble in methanol, ethanol, DMF, and acetonitrile
[Zn (furo)$_2$(2-ammpy)$_2$] (**3**)	140–145	28	DMSO, DMF, slightly soluble in methanol, and acetone
[Zn (furo)$_2$(H_2O)(2,2′-bipy)] (**4**)	226–229	51	DMSO, DMF, slightly soluble in methanol, and acetone
[Zn (furo)$_2$(H_2O)$_2$(4,4′-bipy)] (**5**)	201–202	58	DMSO, DMF, slightly soluble in methanol, and acetonitrile
[Zn (furo)$_2$(1,10-phen)] (**6**)	191–192	49	DMSO, DMF, slightly soluble in methanol and acetone
[Zn (furo)$_2$(2,9-dmp)] (**7**)	261-265[d]	32	DMSO, DMF, slightly soluble in methanol and acetone
[Zn (furo)$_2$(quin)$_2$] (**8**)	198–199	92	DMSO, DMF, slightly soluble in methanol

d: decomposed

3.3 | Infrared spectroscopy

The IR spectra in the range of (200–4000) cm^{-1} was used to characterize the prepared zinc complexes. Table S7 shows the bands assignment and their corresponding wave numbers for Na_{furo} and complex **1**. The IR spectra for complex **1** shows two (COO^-) stretching bands symmetric and asymmetric, v_s (COO^-) at 1383 cm^{-1} and v_{as} (COO^-) at 1605 cm^{-1}. The difference between two bands (Δv (COO^-) = 222 cm^{-1}) which is less than (Δv (COO^-) = 229 cm^{-1}) of Na_{furo} indicates chelating bidentate coordination modes between zinc and furosemide.[62] The v(M-O) and v(M-N) bands for metal complexes occur in the range of (430–520) cm^{-1} and (542–576) cm^{-1} as weak bands, respectively.

Assignments of IR spectral data of complexes (**2–8**) are shown in Tables S8 and S9 (supporting information). In complex **2**; Δv (COO^-) = 233 cm^{-1} is greater than Δv (COO^-) of Na_{furo}, indicating monodentate coordination mode. Also in complex **3**; Δv (COO^-) = 240 cm^{-1} is greater than Δv (COO^-) of Na_{furo}, indicating monodentate coordination mode. In complex **4**; Δv (COO^-) = 225 cm^{-1} is less than Δv (COO-) of Na_{furo}, indicating chelating bidentate coordination mode, but X-ray structure analysis indicates bidentate coordination mode for the first carboxylate group and monodentate for the second, respectively. In complex **5**; Δv (COO) = 191 cm^{-1} is less than Δv (COO^-) of Na_{furo}, chelating bidentate is expected. In complex **6**; Δv (COO^-) = 183 cm^{-1} is less than Δv (COO^-) of Na_{furo}, this also indicates chelating bidentate. In complex **7**; Δv

(COO-) = 208 cm^{-1}, less than Δv (COO_) of Na_{furo}, therefore indicating chelating bidentate coordination mode. In complex **8**; Δv (COO^{-}) = 232 cm^{-1}, greater than Δv (COO^{-}) of Na_{furo}, indicating monodentate coordination mode.[62]

3.4 | Electronic absorption spectroscopy

Metal to ligand transitions (MLCT) primary occur in the (201–296) nm region.[63–65] Table 3 shows no LMCT, because Zn(II) is a d^{10} cation with completely filled d-orbitals. In addition, d-d electronic transition will not happen for the same reason. The origin of the observed bands in complexes (**1–8**) are due to MLCT and intra-ligand transitions. The spectra of the Zn(II) complexes are similar to the spectra of the parent ligands with very small blue or red shifts.

3.5 | X-ray crystallography

Crystal structure of complex **4** was determined and suitable crystal was obtained by recrystalization from MeOH. Crystallographic information files (CIF) may be found online in the supporting information tap of this article.

3.5.1 | X-ray crystal structure of [Zn (furo)$_2$(H_2O)(2,2′-bipy)] (4)

The molecular structure view, atomic numbering scheme and atom connectivity of complex **4** are shown in Figure 3.

The Zn(II) is bound to one monodentate, one bidentate furosemide, one bidentate 2,2′-bipy and one water molecule and formed a distorted octahedral arrangement around the metal center. 2,2′-bipy ligand formed stable five member ring with Zn metal center.

TABLE 3 UV–visible spectral data for the prepared complexes and pure ligand

Complexes	λ_{max} (nm)	Parent ligands	λ_{max} (nm)
[Zn (furo)$_2$] (**1**)	229, 275	Furo	233, 274
[Zn (furo)$_2$(2-ampy)$_2$] (**2**)	234, 296	2-ampy	230, 276
[Zn (furo)$_2$(2-ammepy)$_2$] (**3**)	229, 274	2-ammepy	206, 261
[Zn (furo)$_2$(H_2O)(2,2′-bipy)] (**4**)	230, 276	2,2-bipy	236, 282
[Zn (furo)$_2$(4,4′-dipy)] (**5**)	228, 275	4,4-dipy	204, 241
[Zn (furo)$_2$(1,10-phen)] (**6**)	229, 272	1,10-phen	230, 264
[Zn (furoe)$_2$(2,9-dmp)] (**7**)	229, 275	2,9-dmp	229, 270
[Zn (furo)$_2$(quin)$_2$] (**8**)	204, 225	quin	224, 275

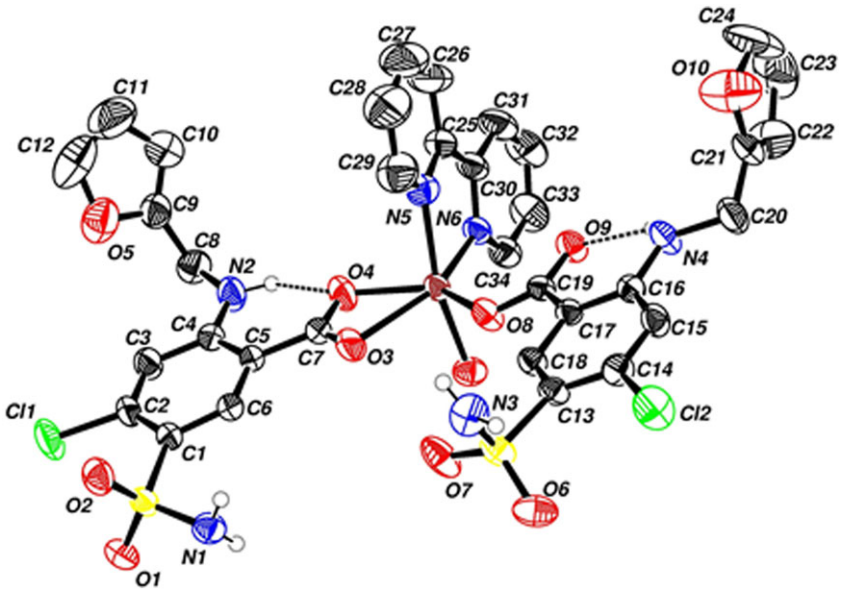

FIGURE 3 Molecular structure view of complex **4** showing the atom labeling scheme

Selected bond distances and bond angles for complex **4** are shown in Table 4.

Hydrogen bonds formation depend on molecular recognition of complementary parts of the molecules containing donor and acceptor groups and molecular stereochemistry. This type of interaction is strongly directional and is used in supra-molecular chemistry and crystal engineering to produce novel (bio) nano-material. Hydrogen bonds play an important role in the stability of crystal structures and therefore can be used in identification of the protein structures, and is a key building block in the DNA formation. The bond formed between –OH of one molecule and the electron lone pair of –N atom of another molecule leads to tight crystal packing.[66–68]

The bond distances of O-Zn (2.336(2) Å, 2.159(2) Å, 1.9912(19) Å and 2.100(2) Å) are similar to previously reported values (1.84–2.33).[69] N-Zn bond distances 2.134(3) Å, and 2.125(2) Å are smaller than previously reported values (2.169–2.197).[70] Complex **4** formed a distorted octahedral geometry around Zn(II) center due to unsymmetrical bond angles. Intra-hydrogen bonds were formed between a lone pair of electrons on one of O(9), O(2), O(4), O(6), O(3), O(7) and a hydrogen atom bonded to one of the N(1), N(2), N(3), N(4) and O(1 W) within the same complex, whereas inter-hydrogen bonds were formed between hydrogen of N(3) and lone pair of electrons of O(1ME) or hydrogen of O(1ME) and lone pair of electrons of O(1) between different molecules. (ME = molecule of methanol solvent of crystallization). Table 5 shows the hydrogen bond distances in (Å) and their angles in (°).

3.6 | Biological activity (*In-vitro*)

Before measurement of their biological activity, the solution stability of the complexes was tested and checked periodically by ^{1}H and ^{13}C NMR in chloroform and DMSO solvents, consistently providing data similar to the stability proved in our previously reported work.[9,16–18,28,29] In addition, the complexes were crystallized by slow solvent evaporation at room temperature which took several days and when checked, the same properties of the compounds were obtained (supplementary materials of Abu Ali and Jabali.[28]

3.6.1 | Anti-bacterial activity

The anti-bacterial activity of complexes (**1**–**8**) were tested using agar diffusion method against gram-positive and gram-negative bacteria. The results are shown in Tables 6 and 7 for gram-negative and gram-positive bacteria, respectively.

Most of the prepared complexes did not show considerable anti-bacterial activity against gram-negative bacteria except complexes **4** and **6**. This minor activity is possibly due to the fact that gram-negative bacteria contain

TABLE 4 Selected bond distances (Å) and bond angles (°) of complex **4**

Bond	Distance (Å)	Bonds	Angle (°)
O(3)-Zn(1)	2.336(2)	N(6)-Zn(1)-O(3)	152.66(8)
O(4)-Zn(1)	2.159(2)	O(4)-Zn(1)-O(3)	57.90(8)
O(8)-Zn(1)	1.9912(19)	O(1 W)-Zn(1)-O(3)	91.14(8)
O(1 W)-Zn(1)	2.100(2)	O(8)-Zn(1)-O(3)	84.04(8)
C(7)-O(3)	1.252(4)	N(5)-Zn(1)-O(4)	94.22(10)
C(7)-O(4)	1.268(4)	N(6)-Zn(1)-O(4)	94.76(9)
C(19)-O(8)	1.261(3)	O(1 W)-Zn(1)-O(4)	93.21(9)
C(19)-O(9)	1.246(3)	O(8)-Zn(1)-O(4)	141.91(8)
N(5)-Zn(1)	2.134(3)	O(8)-Zn(1)-O(1 W)	88.40(9)
N(6)-Zn(1)	2.125(2)	O(8)-Zn(1)-N(6)	123.29(8)
C(29)-N(5)	1.339(5)	O(1 W)-Zn(1)-N(6)	90.55(9)
C(25)-N(5)	1.334(4)	O(8)-Zn(1)-N(5)	92.88(9)
C(30)-N(6)	1.350(4)	O(1 W)-Zn(1)-N(5)	166.22(9)
C(34)-N(6)	1.343(4)	N(6)-Zn(1)-N(5)	77.28(10)
		N(5)-Zn(1)-O(3)	102.64(9)
		C(19)-O(8)-Zn(1)	124.52(17)

TABLE 5 Hydrogen bond distances (Å) and bond angles (°)

D-H...A	d(D-H)	d(H...A)	d(D...A)	<(DHA)
N(1)-H(1AN)...O(9)#1	0.92	1.93	2.841(3)	170.7
N(1)-H(1BN)...O(2)#2	0.87	2.03	2.897(3)	172.6
N(2)-H(2 N)...O(4)	0.87	1.93	2.656(4)	140.4
N(3)-H(3AN)...O(6)#3	0.91	2.16	3.023(4)	159.4
N(3)-H(3BN)...O(1ME)	0.81	2.20	2.984(5)	163.5
N(4)-H(4 N)...O(9)	0.89	1.99	2.703(3)	136.7
O(1 W)-H(1 W)...O(3)#1	0.83	1.93	2.754(3)	172.2
O(1 W)-H(2 W)...O(7)#1	0.85	2.03	2.840(3)	160.2
O(1ME)-H(1ME)...O(1)#2	0.82	2.25	3.000(4)	151.5

Symmetry transformations used to generate equivalent atoms: #1 -x + 1,-y,-z + 1 #2 -x,-y,-z + 1 #3 -x + 1,-y,-z + 2

TABLE 6 *In-vitro* anti-bacterial activity data for complexes (**1–8**) against gram negative bacteria

Compounds	*E. coli*	*P. mirabilis*	*P. aeruginosa*
Gentamycin	13.7 ± 1.2	14.0 ± 1.0	11.7 ± 0.6
Erythromycin	11.3 ± 0.6	9.3 ± 1.2	10.7 ± 1.2
$ZnCl_2$	-	-	-
Furo	-	-	-
DMSO	-	-	-
Complex **1**	-	-	-
Complex **2**	-	-	-
2-ampy	-	-	-
Complex **3**	-	-	-
2-ammepy	-	-	-
Complex **4**	-	10.0 ± 1.0	-
2,2′-bipy	10.3 ± 0.6	13.0 ± 1.0	-
Complex **5**	-	-	-
4,4′-dipy	-	-	-
Complex **6**	11.7 ± 0.6	10.0 ± 1.0	-
1,10-phen	16.0 ± 1.0	19.3 ± 3.2	-
Complex **7**	-	-	-
2,9-dmp	-	-	-
Complex **8**	-	-	-
Quin	-	-	-

Inhibition zone diameter (millimeter (mm)) ± Standard error

TABLE 7 *In-vitro* anti-bacterial activity data for complexes (**1–8**) against gram positive bacteria

Compounds	*S. aureus*	*S. epidemidis*	*B. subtilis*
Gentamycin	13.3 ± 0.6	19.0 ± 3.0	13.7 ± 1.5
Erythromycin	19.3 ± 0.6	20.7 ± 1.2	18.3 ± 1.2
$ZnCl_2$	-	6.3 ± 0.6	-
Furo	-	-	-
Complex **1**	-	-	-
Complex **2**	-	-	-
2-ampy	-	-	-
Complex **3**	-	6.0 ± 1.0	-
2-ammepy	-	-	-
Complex **4**	8.7 ± 1.5	-	-
2,2′-bipy	8.3 ± 0.6	11.7 ± 0.6	9.3 ± 0.6
Complex **5**	8.0 ± 1.4	-	-
4,4′-dipy	-	-	-
Complex **6**	11.7 ± 0.6	13.7 ± 0.6	8.0 ± 0.0
1,10-phen	18.7 ± 1.2	22.0 ± 1.0	16.3 ± 0.6
Complex **7**	8.0 ± 0.0	11.3 ± 0.6	8.7 ± 0.6
2,9-dmp	11.0 ± 0.0	16.3 ± 0.6	7.0 ± 1.0
Complex **8**	-	-	-
Quin	-	-	-

Inhibition zone diameter (millimeter (mm)) ± Standard error

cytoplasmic inner membrane and an outer membrane that contains lipopolysaccharide molecules. The space between the two membranes contains peptidoglycan cell wall and many unique proteins where the outer membrane acts as a protective membrane preventing the noxious compounds from reaching the cell.[71] Complex **4** showed anti-bacterial activity against *p.mirabilis* with IZD equals 10.0 mm and complex **6** showed anti-bacterial activity against *E. coli and P. mirabilis* with IZD equals 11.7 mm and 10.0 mm, respectively. The parent ligand 2,2′-bipy shows higher anti-bacterial activity against *P.mirabilis* with IZD equals 13.0 mm compared to complex **4**. Also 2,2′-bipy shows anti-bacterial activity against *E. coli* with IZD equals 10.3 mm, but complex **4** didn't show any anti-bacterial

activity against this type of gram negative bacteria. In addition, 1,10-phen shows higher anti-bacterial activity against *E. coli* and *P. mirabilis* compared to complex **6** with IZD equals 16.0 mm and 19.3 mm, respectively.

The anti-bacterial activity for complexes **4** and **6** is lower than G, but higher than E against *P. mirabilis*. Also complex **6** has slightly higher anti-bacterial activity than E, but lower than G against *E. coli*.

In the case of gram positive bacteria, more of the prepared complexes show anti-bacterial activity when compared with gram negative bacteria as presented in Table 7.

$ZnCl_2$, furo, and Complexes **1**, **2** and **8** didn't show any anti-bacterial activity against gram-negative and gram-positive bacteria except $ZnCl_2$ showed very low anti-bacterial activity against *S. epidermidis* with IZD equals 6.3 mm.

Complex **3** showed low anti-bacterial activity against *S. epidermidis* with IZD equals 6.0 mm and this value is lower than values of G and E. Complex **4** only showed anti-bacterial activity against *S. aureus* with IZD equals 8.7 mm and this value is very low when compared with G and E while the parent ligand 2,2′-bipy showed higher anti-bacterial activity against all tested microorganisms.

Complex **5** showed anti-bacterial activity against *S. aureus* with IZD equals 8.0 mm and this value is lower than values of G and E, the parent ligand didn't show anti-bacterial activity against any types of gram positive bacteria. Complex **6** showed anti-bacterial activity against all tested gram-positive bacteria (*S. aureus, B. subtilis, S. epidermidis*) with IZD equals 11.7 mm, 8.0 mm, and 13.7 mm, respectively. These values are lower than values of G and E, however the parent ligand 1,10-phen showed higher anti-bacterial activity than complex **6** for all tested bacteria.

Complex **7** showed anti-bacterial activity for all type of gram-positive bacteria (*S. aureus, B. subtilis, S. epidermidis*) with IZD equal 8.0 mm, 8.7 mm, and 11.3, respectively and these values are lower than values of G

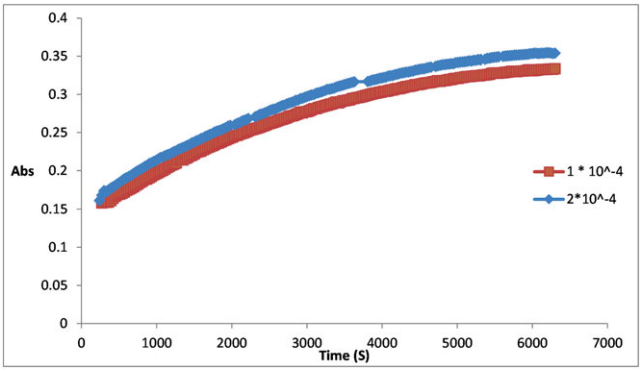

FIGURE 4 Caption: BNPP hydrolysis at different concentrations of complex **7** in DMSO/HEPES buffer solution under certain conditions ([BNPP] = 1 x 10^{-4} M, pH = 7.00 and temp = 25 °C)

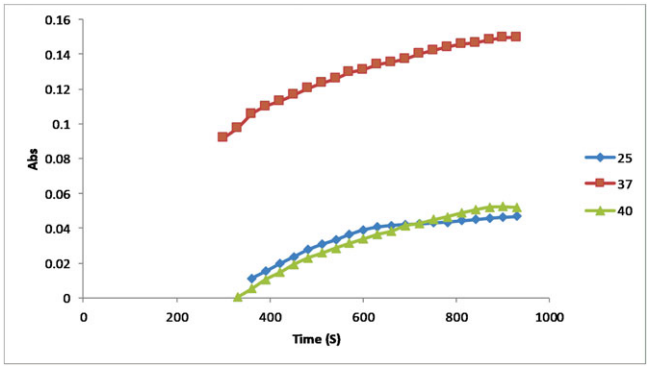

FIGURE 5 BNPP hydrolysis at different temperature values in DMSO/HEPES buffer solution under certain conditions ([BNPP] = 1 x 10^{-4} M, [complex **4**] = 2 x 10^{-4} M, and pH = 7.00)

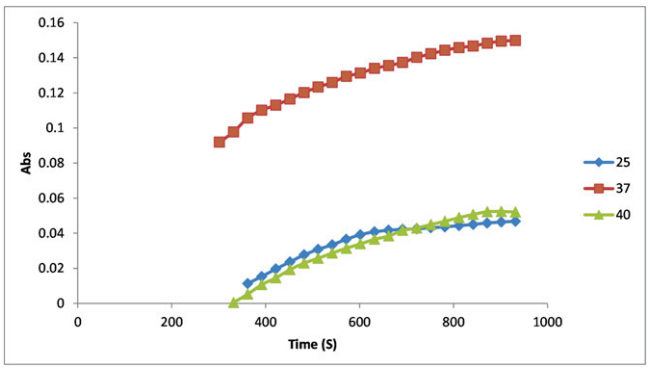

FIGURE 6 BNPP hydrolysis at different pH values in DMSO/HEPES buffer solution under certain conditions([BNPP] = 1 x 10^{-4} M, [complex **4**] = 2 x 10^{-4} M and temp = 37 °C)

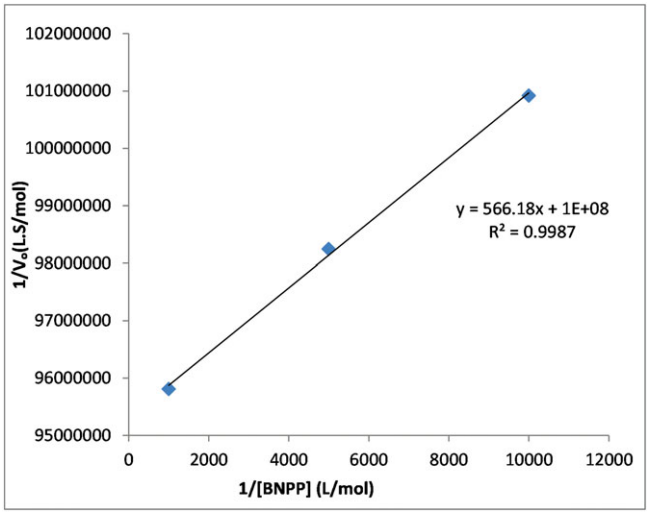

FIGURE 7 Second order rate for complex 4 with different BNPP concentrations under certain conditions (pH =7.00, temp = 37 °C and [complex **4**] = 2 × 10^{-4} M)

and E while the parent ligand 2,9-dmp showed higher anti-bacterial activity compared to complex **7** except *B. subtilis* were it showed slightly higher anti-bacterial activity than its parent ligand.

The stoichiometric ratio of the parent ligands 1,10-phen and 2,9-dmp in complexes **6** and **7** is 19.9% and 22.4% respectively since their contribution in the complex is equivalent to about 20% of the parent ligands. This means that complex formation enhanced the anti-bacterial activity of these parent ligands when compared to free parent ligand. The complexation of zinc furosemide with nitrogen donor ligands showed lower inhibition activity against gram-positive bacteria compared to the positive controls (E and G).

Destructions of bacterial cell walls of *S. aureus* by Zn(II) ion is due to the inhibition of peptidoglycan elongation by the activations of peptidoglycan autolysins of amidases, but the destruction of *E. coli* cell wall is caused by damage of outer membrane structure by degradative enzymes of lipoproteins at N- and C- terminals, the inhibition of peptidoglycan elongation in this type of bacteria depends on the activation of peptidoglycan hydrolases and autolysins of amidase and carboxypeptidase-transpeptidase. DNA damages may be due to Zn ion complex formation by Zn^{2+} substitution into hydrogen bonds in DNA.[72] The anti-microbial activity of metal complexes depend on many factors: (1) the chelate effect of the ligands; (2) the nature of the N-donor ligands; (3) the total charge of the complex; (4) the existence and the nature of the ionic complex; and (5) the nuclearity of the metal center in the complex. In complexes (**1**–**8**) the chelating effect of the ligand is only present. This factor may be the main reason for the diverse anti-bacterial activities which were shown by the complexes.[73]

TABLE 8 Kinetic parameters of BNPP hydrolysis for complexes (**1**–**8**) with different concentration of BNPP

Concentration of complexes (M)		Concentration of BNPP (M)	V_o (mol/L.S)	V_{max} (mol/L.S)	K_m (mol/L)	K_{cat}^{*} (S^{-1})	2-order rate $K_{BNPP}^{\#}$ (L/mol. S)
1	(2×10^{-4})	1×10^{-3}	6.84×10^{-9}	1.00×10^{-8}	1.20×10^{-4}	5.00×10^{-5}	0.42
1	(2×10^{-4})	2×10^{-4}	5.01×10^{-9}	1.00×10^{-8}	1.20×10^{-4}	5.00×10^{-5}	0.42
1	(2×10^{-4})	1×10^{-4}	3.92×10^{-9}	1.00×10^{-8}	1.20×10^{-4}	5.00×10^{-5}	0.42
2	(2×10^{-4})	1×10^{-3}	1.01×10^{-8}	1.11×10^{-8}	6.06×10^{-5}	5.55×10^{-5}	0.91
2	(2×10^{-4})	2×10^{-4}	8.24×10^{-9}	1.11×10^{-8}	6.06×10^{-5}	5.55×10^{-5}	0.91
2	(2×10^{-4})	1×10^{-4}	6.76×10^{-9}	1.11×10^{-8}	6.06×10^{-5}	5.55×10^{-5}	0.91
3	(2×10^{-4})	1×10^{-3}	6.98×10^{-9}	1.00×10^{-8}	1.01×10^{-4}	5.00×10^{-5}	0.49
3	(2×10^{-4})	2×10^{-4}	5.53×10^{-9}	1.00×10^{-8}	1.01×10^{-4}	5.00×10^{-5}	0.49
3	(2×10^{-4})	1×10^{-4}	4.13×10^{-9}	1.00×10^{-8}	1.04×10^{-4}	5.00×10^{-5}	0.49
4	(2×10^{-4})	1×10^{-3}	1.04×10^{-8}	1.00×10^{-8}	5.66×10^{-6}	5.00×10^{-5}	8.83
4	(2×10^{-4})	2×10^{-4}	1.01×10^{-8}	1.00×10^{-8}	5.66×10^{-6}	5.00×10^{-5}	8.83
4	(2×10^{-4})	1×10^{-4}	9.90×10^{-9}	1.00×10^{-8}	5.66×10^{-6}	5.00×10^{-5}	8.83
5	(2×10^{-4})	1×10^{-3}	9.33×10^{-9}	1.00×10^{-8}	5.08×10^{-5}	5.00×10^{-5}	0.98
5	$(2 \times 10^{-4)}$	2×10^{-4}	8.05×10^{-9}	1.00×10^{-8}	5.08×10^{-5}	5.00×10^{-5}	0.98
5	(2×10^{-4})	1×10^{-4}	6.55×10^{-9}	1.00×10^{-8}	5.08×10^{-5}	5.00×10^{-5}	0.98
6	(2×10^{-4})	1×10^{-3}	6.78×10^{-9}	1.00×10^{-8}	5.39×10^{-5}	5.00×10^{-5}	0.93
6	(2×10^{-4})	2×10^{-4}	5.82×10^{-9}	1.00×10^{-8}	5.39×10^{-5}	5.00×10^{-5}	0.93
6	(2×10^{-4})	1×10^{-4}	4.97×10^{-9}	1.00×10^{-8}	5.39×10^{-5}	5.00×10^{-5}	0.93
7	(2×10^{-4})	1×10^{-3}	8.28×10^{-9}	1.00×10^{-8}	4.24×10^{-5}	5.00×10^{-5}	1.17
7	(2×10^{-4})	2×10^{-4}	7.24×10^{-9}	1.00×10^{-8}	4.24×10^{-5}	5.00×10^{-5}	1.17
7	(2×10^{-4})	1×10^{-4}	6.29×10^{-9}	1.00×10^{-8}	4.24×10^{-5}	5.00×10^{-5}	1.17
8	(2×10^{-4})	1×10^{-3}	11.72×10^{-9}	1.00×10^{-8}	4.57×10^{-5}	5.00×10^{-5}	1.09
8	(2×10^{-4})	2×10^{-4}	7.23×10^{-9}	1.00×10^{-8}	4.57×10^{-5}	5.00×10^{-5}	1.09
8	(2×10^{-4})	1×10^{-4}	6.41×10^{-9}	1.00×10^{-8}	4.57×10^{-5}	5.00×10^{-5}	1.09

(*) $K_{cat} = V_{max}/[complex]$, (#) $K_{BNPP} = K_{cat}/K_m$

Although it is not clear why some compounds exhibit different bacterial activity with Gram-positive and Gram-negative bacteria, it may be ascribed to the difference in the overall structure of their cell walls.[30,74] Metal ions are essential for the survival of microbes in the environment or the host. Therefore, the microbes should ensure uptake of metal ions according to their physiological needs as the imbalance in metals homeostasis could be deleterious to the microbe. Host defense against bacterial infection consists of either sequestering ions resulting in bacterial starvation, or increased release of these metals, which results in toxicity.[30]

3.7 | BNPP catalytic hydrolysis

All zinc furosemide complexes were tested for their catalytic activity in BNPP hydrolysis. The rate of BNPP hydrolysis was performed at different temperatures, pH values and different concentrations. The optimum conditions for BNPP hydrolysis were determined by varying one of the above factors and keeping the other two factors constant.

3.7.1 | Effect of concentration on the BNPP hydrolysis

Figure 4 shows the relationship between absorbance and time at different concentration of complex **7** and constant temp, pH and concentration of BNPP. The initial rates were determined to be 3.8 x 10^{-9} and 5.6 x 10^{-9} mol/L.s for 1 x 10^{-4} M and 2 x 10^{-4} M, respectively. By measuring the absorbance of p-nitrophenol vs. time at 400 nm, the initial rate of BNPP hydrolysis can be determined.

3.7.2 | Effect of temperatures on BNPP hydrolysis

The absorbance vs. time for complex **4** is plotted in Figure 5 at different temperature values while pH, concentrations of BNPP and complex were maintained constant. The values of initial rates at 25 °C, 37 °C, and 40 °C were determined to be 8.6 x 10^{-9}, 9.9 x 10^{-9}, and 9.2 x 10^{-9} (mol/L.s) respectively with maximum initial rate observed at 37 °C for complex **4**.

3.7.3 | Effect of pH on BNPP hydrolysis

Figure 6 shows the relationship between absorbance and time for complex **4** at different pH values and a temperature of 37 °C and constant concentration of both BNPP and complex. The initial rate values 9.9 x 10^{-9}, 6.4 x 10^{-9}, and 7.8 x 10^{-9} (mol/L.s) were obtained for pH = 7.00, 7.54, and 7.92, respectively. The maximum initial rate value for catalytic activity of complex **4** on the hydrolysis of BNPP was observed at pH = 7.00.

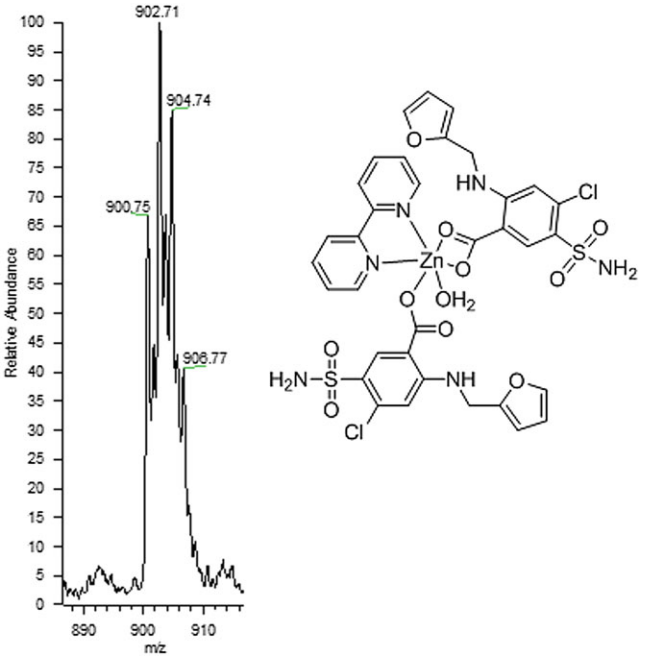

FIGURE 8 ESI-MS spectra of complex **4**

Figure 7 shows the relationship between the reciprocal of the concentration of BNPP and rate of hydrolysis for complex **4** according to Michaelis- Menten equation ($1/V_o = 1/V_{max} + K_m/V_{max}$ [BNPP]).[75] All complexes (**1**–**8**) have the similar relationship and the kinetic parameters of BNPP hydrolysis shown in Table 8 are closely related and comparable to previously reported values.[22,30,76–78] One of the possible mechanisms is proposed in our and others previous publications.[22,30,76–78]

The rate of BNPP hydrolysis using complexes as catalysts was in the following order: complex **4** > **2** > **5** > **8** > **7** > **6** > **3** > **1**.

3.8 | Mass spectrometry

Figures S1-S8 (supporting information) show the ESI-MS spectra of all complexes (**1**–**8**). As an example, the average molecular weight of complex **4** is equal to 901 amu as shown in Figure 8.

4 | CONCLUSIONS

The prepared zinc complexes with furosemide in the presence of N-donor ligands were synthesized and characterized using the different techniques of IR, UV–Vis, ^{1}H NMR, ^{13}C NMR, LC/MS and others. Complexes **4** and **6** showed anti-bacterial activity against *P. mirabilis*

with Inhibition Zone Diameter (IZD) equals 10.0 mm and complex **6** showed anti-bacterial activity against *E. coli* with IZD equals 11.7 mm. Regarding gram-positive bacteria, only complex **3** showed low anti-bacterial activity against *S. epidermidis* with IZD equals 6.0 mm. Complexes **4** and **5** showed anti-bacterial activity against *S. aureus* with IZD equals 8.7 mm and 8.0 mm, respectively.

Complex **7** showed anti-bacterial activity against all types of gram-positive bacteria (*S. aureus, B. subtilis, S. epidermidis*) with IZD equals 8.0 mm, 8.7 mm and 11.3 mm, respectively. The single-crystal structure of Complex **4** revealed distorted octahedral geometry with one bidentate furosemide carboxylate group, one monodentate furosemide carboxylate, one bidentate 4,4-bipy, and one water molecule.

The rate of BNPP hydrolysis was tested in order to determine the effect of zinc complexes on the phosphates hydrolysis. The results showed that the hydrolysis rate of BNPP was in the following order: **4 > 2 > 5 > 8 > 7 > 6 > 3 > 1** for the tested complexes.

ACKNOWLEDGEMENT

The authors thank the office of Vice President for Academic Affairs at Birzeit University for their financial support.

ORCID

Hijazi Abu Ali http://orcid.org/0000-0002-6315-6868

REFERENCES

[1] K. Soetan, C. Olaiya, O. Oyewole, *Afr. J. Food Sci.* **2010**, *4*, 200.

[2] J. Glusker, A. Katz, C. Bock, *The Rigaku Journal* **1999**, *16*, 8.

[3] C. Livingstone, *Nutr. Clin. Pract.* **2015**, *371*.

[4] S. Frassinetti, C. Croce, *J. Environ. Pathol. Toxicol. Oncol.* **2006**, *25*, 597.

[5] J. Osredkar, N. Sustar, *J. Clin. Toxicol.* **2011**, *S3*, 001.

[6] M. Selvaganapathy, N. Raman, *J. Chem. Biol. Ther.* **2016**, *1*, 1.

[7] A. Ravasio, L. Boggioni, I. Tritto, *Olefin Upgraing Catalysis by Nitrogen–based Metal Complexes*, Vol. 27 **2011**.

[8] Z. Bujdosova, K. Gyoryova, J. Kovarova, D. Hudecova, L. Halas, *J. Therm. Ana. Calorim.* **2009**, *98*, 151.

[9] H. Abu Ali, M. Darawsheh, A. Abuhijleh, E. Rappoccioio, M. Akkawi, S. Jaber, S. Maloul, Y. Hussein, *Eur. J. Med. Chem.* **2014**, *82*, 152.

[10] N. Kumar, P. A. V. G. S, *Int. J. Basic Appl. Chem. Sci.* **2015**, *5*, 52.

[11] A. L. Abu Hijleh, H. Abu Ali, A. Emwas, *J. Org. Chem.* **2009**, *694*, 3590.

[12] E. Szunyogova, K. Gyoryova, D. Hudecova, L. Piknova, J. Chomic, Z. Vargova, V. Zelenak, *J. Therm. Anal. Calorim.* **2007**, *88*, 220.

[13] M. C. Rodriguez-Arguelles, S. Mosquera-Vazquez, J. Sanmartin-Matalobos, A. M. Garcia-Deibe, C. Pelizzi, F. Zani, *Polyhedron* **2010**, *867*.

[14] V. Zeleňák, Z. Vargová, K. Györyová, *Spectrochim. Acta A: Molecular and Biomolecular Spectroscopy* **2007**, *66*, 262.

[15] J. E. Weder, C. T. Dillon, T. W. Hambley, B. J. Kennedy, P. A. Lay, J. R. Biffin, H. L. Regtop, N. M. Davies, *Coord. Chem. Rev.* **2002**, *232*, 95.

[16] H. Abu Ali, M. Darweesh, E. Rappocciolo, *Polyhedron* **2013**, *61*, 235.

[17] H. Abu Ali, H. Fares, M. Darweesh, E. Rappocciolo, M. Akkawi, S. Jaber, *Eur. J. Med. Chem.* **2015**, *89*, 67.

[18] B. Jabali, H. Abu Ali, *Polyhedron* **2016**, *117*, 249.

[19] H. Abu Ali, S. Maloul, I. Abu Ali, M. Akkawi, S. Jaber, *J. Coord. Chem.* **2514**, *2016*, 69.

[20] H. Abu Ali, A. Abu Shamma, S. Kamel, *J. Mol. Struct.* **2017**, *1142*, 40.

[21] H. Abu Ali, A. Shalash, M. Akawi, S. Jaber, *Appl. Organomet. Chem.* **2017**, *31*, 11. https://doi.org/10.1002/aoc.3772

[22] A. Abu Shamma, H. Abu Ali, S. Kamel, *Appl. Organomet. Chem.* **2017**, *32*. https://doi.org/10.1002/aoc.3904

[23] A. Shalash, H. Abu Ali, *Chem. Cent. J.* **2017**, *11*, 40.

[24] S. Kamel, H. Abu Ali, A. Abu Shamma, *J. Coord. Chem.* **2017**, *70*, 1910. https://doi.org/10.1080/00958972.2017.1326593

[25] S. Omar, H. Abu Ali, *J. Coord. Chem.* **2017**, *70*, 2436.

[26] N. Palanisami, P. Rajakannu, R. Murugavel, *Inorg. Chim. Acta* **2013**, *405*, 522.

[27] S. Baca, *Int Res J Pure Appl Chem* **2012**, *2*, 1.

[28] H. Abu Ali, B. Jabali, *Polyhedron* **2016**, *16*, 1.

[29] H. Abu Ali, S. Omar, M. Darawsheh, H. Fares, *J. Coord. Chem.* **2016**, *69*, 1110.

[30] H. Abu Ali, S. Kamel, A. Abu Shamma, *Appl. Organomet. Chem.* **2017**, *31*. https://doi.org/10.1002/aoc.3829

[31] G. Granero, M. Longhi, H. Mora, K. Junginger, V. Midha, S. Shah, S. Stavchansky, J. Dressman, D. Barends, *J. Pharm. Sci.* **2009**, *99*, 2544.

[32] P. C. Rowbotham, J. B. Stanford, J. K. Sugden, *Pharm. Acta Helv.* **1976**, *51*, 304.

[33] S.-C. Shin, J. Kim, *Int. J. Pharm.* **2003**, *251*, 79.

[34] A. Lebedev, L. Mironova, I. Pleshakov, *Pharm. Chem. J.* **1985**, *19*, 697.

[35] I. Al Omar, R. Al Shban, A. Shah, *Res. J. Pharmacol.* **2009**, 363.

[36] J. Lahet, F. Lenfant, C. Courderot-Masuyer, E. Ecarnot-Laubriet, C. Vergely, M. Durnet-Archeray, M. Freysz, L. Rochette, *Life Sci.* **2003**, *73*, 1075.

[37] V. Hondrellis, T. Kabanos, S. Perlepes, J. Tsangaris, *Monatsh. Chem.* **1988**, *119*, 1091.

[38] W. Lustri, S. Lazarini, B. Lustri, P. Corbi, M. Silva, F. Nogueira, O. Filho, A. Massabni, H. Barud, *J. Mol. Struct.* **2016**, 1.

[39] A. Gölcü, *J. Anal. Chem.* **2006**, *61*, 784.

[40] P. Pontchev, H. Kadum, G. Gochev, B. Evtimova, *Polyhedron* **1992**, *11*, 1973.

[41] L. Zivanović, S. Agatonović, D. Radulović, *Microchim. Acta* **1990**, *100*, 49.

[42] Y. Liu, H. Wang, J. Wang, Y. Li, *Lumin. J. Biol. Chem. Lumin.* **2012**, *28*, 882.

[43] M. Valle-Orta, D. DÍaz, I. Dubé, J. Quiñonez, R. Guerrero, *J. Phys.* **2017**, *838*, 1.

[44] M. Young, *Faculty of Graduate Studies and Research Phosphate Diester Cleavage Mediated by Transition Metal Complexes*, Mc Gill University **1996**.

[45] J. Floriá, A. Warshel, *J. Phys. Chem. B* **1998**, *102*, 719.

[46] W. Jiang, B. Xu, Q. Lin, J. Li, F. Liu, X. Zeng, H. Chem, *Collids Surfaces A: Physicochem. Eng. Aspects* **2008**, *315*, 103.

[47] W. Jiang, B. Xu, J. Zhong, J. Li, F. Liu, *J. Chem. Sci.* **2008**, *120*, 411.

[48] J. Xie, C. Li, M. Wang, B. Jiang, *Chem. Pap.* **2013**, *67*, 365.

[49] J. Xie, B. Jiang, X. Kou, C. Hu, X. Zeng, *Transit. Met. Chem.* **2003**, *28*, 782.

[50] J. Li, H. Li, B. Zhou, W. Zeng, S. Qin, *Transit. Met. Chem.* **2005**, *30*, 278.

[51] Z. S. Zhang, X. M. Yu, X. M. J. K. Fong, L. D. Margerum, *Inorg. Chim. Acta* **2001**, *317*, 72.

[52] K. Dong, M. Xiang-Guang, J. Ying Liu, J. Du, K. Xing-Ming, Z. Xian-Cheng, *Physiochem. Eng. Aspects* **2008**, *324*, 189.

[53] F. Jiang, J. Du, X. Yu, J. Bao, X. Zeng, *J. Colloid Interface Sci.* **2004**, *273*, 497.

[54] J. Florián, A. Warshel, *J. Phys. Chem. B* **1998**, *4*, 719.

[55] L. Jian-zhang, L. Hong-bo, Z. Bo, Z. Wei, Q. Sheng-ying, J. X. Shen-xin Li, *Transit. Met. Chem.* **2005**, *3*, 278.

[56] SMART-NT V5.6, B. A. G., D-76181 Karlsruhe, Germany, **2002**.

[57] SAINTL-NT V5.0, B. A. G., D-76181 Karlsruhe, Germany, **2002**.

[58] SHELXTL-NT V6.1, B. A. G, D-76181 Karlsruhe, in *Germany*, **2002**.

[59] A. Rahman, M. L. Choudhary, W. J. Thomsen, *Bioassay techniques for drug development*, Harwood Academic, Amsterdam **2001**.

[60] A. Abuhijleh, *Polyhedron* **1997**, *16*, 733.

[61] J. Torres, M. Brusoni, F. Peluffo, C. Kremer, S. Domínguez, A. Mederos, E. Kremer, *Inorg. Chim. Acta* **2005**, *358*, 3320.

[62] K. Nakamoto, *Infrared and Raman spectra of inorganic and coordination compounds*, 6th ed., Wiley, Hoboken, N. J **2009**.

[63] X. Zhang, Z.-h. Yi, M. Xue, Y. Xu, J. h. Yu, X.-Y. Yu, J.-Q. Xu, *Chem. Res. Chin. Univ.* **2007**, *23*, 631.

[64] H.-l. Yu, J. Yang, Q. Fu, J.-c. Ma, W.-l. Li, *Chem. Res. Chin. Univ.* **2008**, *24*, 123.

[65] S. Xin-Min, W. Hai-Yan, L. Yan-Bing, Y. Jing-Xin, C. Lei, H. Ge, X. Wei-Ging, Z. Bing, *Chem. Res. Chin. Univ.* **2010**, *26*, 1011.

[66] A. Cruz Cabeza, G. Day, W. Samual Motherwell, W. Jones, *Cryst. Growth Des.* **2007**, *7*, 100.

[67] B. Kojić-Prodić, K. Molčanov, *Acta Chim. Slov.* **2008**, *55*, 692.

[68] H. Saluja, A. Mehanna, R. Panicucci, E. Atef, *Molecules* **2016**, *21*, 1.

[69] A. Shalash, H. Abu Ali, Faculty of Graduate Studies, Non-steroidal Zn (II) and Co (II) Sulindac Drugs and Bioactive bacterial Effect, Anti-malarial Effect and The Use as Phosphate Hydrolyzing Enzymes, Birzeit University, **2015**.

[70] Y. Yadav, T. Mastropietro, E. Szerb, A. Talarico, S. Pirillo, D. Pucci, A. Crispini, M. Ghedini, *New J. Chem.* **2013**, *37*, 1486.

[71] H. Nikaido, T. Nakae, *Adv. Microb. Physiol.* **1980**, *20*, 163.

[72] T. Ishida, *J. Genes Proteins* **2017**, *1*, 1.

[73] E. Efthimiadou, Y. Sanakis, N. Katsaros, A. Karaliota, G. Psomas, *Polyhedron* **2007**, *26*, 1148.

[74] S. G. K. Atmaca, R. Çicek, *Turk J Med Sci.* **1998**, *28*, 595.

[75] A. Abu Shamma, H. Abu Ali, Faculty of Graduate Studies, New mixed ligand Cobalt (II/III) complexes based on the drug sodium valproate and bioactive Nitrogen-donor ligands. Synthesis, structure and biological properties. Birzeit University, **2016**.

[76] J. Li, H. Li, B. Zhou, W. Zeng, S. Qin, S. Li, J. Xie, *Transit. Met. Chem.* **2005**, *30*, 278.

[77] K. Dong, Y. L. Xiang-Guang, D. Juan, X.-C. Z. Xing-Ming Kou, *Coll Surf A Physicochem. Eng. Asp.* **2008**, *324*, 189.

[78] W. Jiang, B. Xu, J. Zhong, J. Li, F. Liu, *J. Chem. Sci.* **2008**, *120*, 411.

SUPPORTING INFORMATION

Additional supporting information may be found online in the Supporting Information section at the end of the article.

How to cite this article: Raymoni G, Abu Ali H. Synthesis, Structures and Various Biological Applications of New Zn(II) Complexes Having Different Coordination Modes Controlled by the Drug Furosemide in Presence of Bioactive Nitrogen Based Ligands. *Appl Organometal Chem*. 2018; e4680. https://doi.org/10.1002/aoc.4680